ICAS 2016

30th Congress of the International Council
of the Aeronautical Sciences
DCC, Daejeon, Korea ; September 25-30, 2016

APPLYING REQUIRED NAVIGATION PERFORMANCE CONCEPT FOR TRAFFIC MANAGEMENT OF SMALL UNMANNED AIRCRAFT SYSTEMS

Jaewoo Jung, Sarah N. D'Souza, Marcus A. Johnson*, Abraham K. Ishihara, Hemil C. Modi**, Ben Nikaido, Hashmatullah Hasseeb***
*NASA Ames Research Center, **SGT Inc., ***Science & Technology Corp.

Keywords: *unmanned aircraft system, traffic management, required navigation performance*

Abstract

In anticipation of a rapid increase in the number of civil Unmanned Aircraft System (UAS) operations, NASA is researching prototype technologies for a UAS Traffic Management (UTM) system that will investigate airspace integration requirements for enabling safe, efficient low-altitude operations. One aspect a UTM system must consider is the correlation between UAS operations (such as vehicles, operation areas and durations), UAS performance requirements, and the risk to people and property in the operational area. This paper investigates the potential application of the International Civil Aviation Organization's (ICAO) Required Navigation Performance (RNP) concept to relate operational risk with trajectory conformance requirements. The approach is to first define a method to quantify operational risk and then define the RNP level requirement as a function of the operational risk. Greater operational risk corresponds to more accurate RNP level, or smaller tolerable Total System Error (TSE). Data from 19 small UAS flights are used to develop and validate a formula that defines this relationship. An approach to assessing UAS RNP conformance capability using vehicle modeling and wind field simulation is developed to investigate how this formula may be applied in a future UTM system. The results indicate the modeled vehicle's flight path is robust to the simulated wind variation, and it can meet RNP level requirements calculated by the formula. The results also indicate how vehicle-modeling fidelity may be improved to adequately verify assessed RNP level.

1 Introduction

In the past decade, interest in civil applications of Unmanned Aircraft System (UAS), such as infrastructure inspection, crop monitoring, emergency response, goods delivery, and entertainment, has grown [1-6]. A 2016 study [7] estimated the addressable market value of these applications at US$127 billion, and found that there are more than 200 manufacturers currently producing civil UAS to meet the global demand. In the United States alone, about 400,000 UAS were sold during 2015 for civil use, and more than 1 million UAS are expected to be sold in 2016 [8]. To address the challenge of ensuring safety with growing UAS operations, the Federal Aviation Administration (FAA) announced Federal Aviation Regulations Small Unmanned Aircraft Rule (FAR Part 107) that allows for the routine use of UAS that weigh less than 25 kg under a set of conditions [9]. As the initial step, the FAA's rule limits flights to daylight and Visual-Line-Of-Sight (VLOS) operations. However, less restricted operations are expected to be allowed in the future, facilitated by advances in UAS technologies and increased insight into operational safety and privacy issues, leading to an exponential growth of the number of operations [10, 11].

Anticipating a rapid increase in the number of UAS operations, NASA is researching prototype technologies for a UAS Traffic Management (UTM) system and airspace integration requirements that will enable safe, efficient low-altitude operations [12]. In a potential UTM system architecture, information about UAS operations, (e.g., vehicles, planned

operational areas and durations), airspace constraints (e.g., Temporary Flight Restrictions), and data to support safe airspace operations (e.g., terrain and obstacle information and low altitude wind forecast), are made available to UAS operators and the general public. One area of investigation is the relation between UAS performance requirements and the risk to people and property in the operational area [13]. For example, requirements for command and control radio link redundancy, aircraft position report accuracy, and trajectory conformance would be more stringent for goods delivery in urban areas than for pipeline inspections in remote areas because of the differences in potential risk to people and property in the operational areas.

The focus of this paper is the development of a quantitative framework to correlate operational risk with trajectory conformance requirements, where the International Civil Aviation Organization's (ICAO) Required Navigation Performance (RNP) concept is applied to specify the latter. RNP is a type of navigation specification that defines the required accuracy for lateral flight path [14], and aircraft conducting RNP operations must remain within that lateral accuracy for 95 percent of the trajectory [15]. RNP is used widely in commercial aviation to reduce air traffic congestion, decrease aviation fuel consumption, and protect the environment [14].

The approach to developing this framework consisted of defining a method to quantify operational risk and, then, defining RNP level as a function of the operational risk. In this framework, greater operational risk corresponds to a more accurate RNP level or, equivalently, to a smaller tolerable Total System Error (TSE). Data and operational constraints from a flight test of a preliminary UTM system prototype are used to provide rationale for a formula that defines this relationship. To facilitate application of this relation in traffic management, an approach is developed to assess small UAS RNP level based on a vehicle model and a wind field generated using Computational Fluid Dynamics (CFD). The results lead to a recommendation of steps that can be taken to

increase vehicle-modeling fidelity and to verify assessed RNP level.

2 Application of RNP in Small UAS Traffic Management

2.1 Brief Overview of RNP and TSE

RNP is a type of Performance-Based Navigation (PBN) specification [14]. It is a method of navigation that permits aircraft operation on any desired flight path within the coverage of ground- or space-based navigation aids, or within the navigational capability of self-contained aids such as Inertial Navigation System (INS), or within the coverage and the navigational capability of the two. RNP specification includes onboard performance monitoring and alerting capability [15].

The lateral accuracy value of RNP is typically specified in the format of the acronym "RNP" followed by the distance in nautical miles (NM) from the intended flight path centerline (e.g., RNP 10 indicates 10NM lateral accuracy). All aircraft conducting RNP operations must have position error of less than the specified distance for 95 percent of the trajectory [16]. This position error is the displacement perpendicular to desired path, and it consists of the following three errors: Navigation System Error (NSE), Flight Technical Error (FTE), and Path Definition Error (PDE). These three errors are assumed to be independent, normally distributed with zero mean, and their sum is Total System Error (TSE) [14]. Fig. 1 illustrates the components of the RNP path error definition. Aircraft
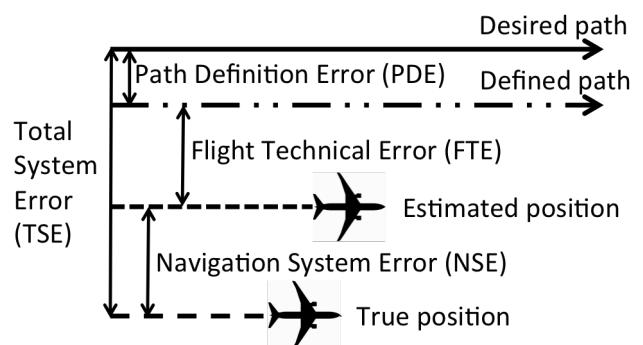

Figure 1. Components of RNP path error

manufacturers typically use statistical test results of flight data, including TSE statistics, for certifying RNP systems (e.g., 95th percentile TSE of 10NM for RNP 10) [16].

2.2 A Heuristic Relation between Operational Risk and RNP Level

Safe integration of UAS into the National Airspace System (NAS) requires a clear understanding of UAS operational risk to other airspace users and persons and property on the surface [17]. However, risk is difficult to quantify because it involves many different variables, ranging from technological failures to human factors [18, 19]. In this paper, the risk of a UAS operation, ξ, is quantified with data from test of a preliminary UTM system prototype, listed in Table 1. The following simplifying assumptions are used.

- Densities of people, properties, and airborne users in the operational area are assumed known and distributed uniformly. The sum of these densities is denoted by $\rho\_vulnerability$, (1), and intended as a single quantity to represent people and assets that are vulnerable to contact with UAS.
- Quantity $\rho\_vulnerability$ is assumed constant throughout the operation.
- Vehicle failures and operational blunders are implicitly incorporated. Risk exposure is defined as being proportional to the duration of the operation.
- The UAS's Kinetic Energy, KE, (2), is used to assess its impact on people and assets.

With these assumptions, risk ξ is defined in (3) with a unit of J•s/m^2.

Table 1. Preliminary UTM system prototype data

Variable Name	Description
Area_boundary	Boundary of the operational area
MTOW	UAS Max. Takeoff Weight (kg)
V_{max}	UAS Max. speed (m/s)
dT	Duration of operation (s)

$$\rho\_vulnerability = \rho\_people + \rho\_property + \rho\_airborne\_user \quad (1)$$

$$KE = 0.5 * MTOW * V_{max}{}^2 \quad (2)$$

$$\xi = \rho\_vulnerability * KE * dT \quad (3)$$

One way to interpret quantity ξ is to use the concept of *Action Density*, *AD*. *Action* is calculated by multiplying *KE* with *dT,* and is "an abstract quantity that describes the overall motion of a physical system" [21]. *AD* is calculated by multiplying *Action* with the densities of people, properties, and airborne users in the operational area, $\rho\_vulnerability$. Therefore, increase in *AD* indicates increased UAS movement over the operational area or increase in the potential impact on people and assets in that area, or both.

To relate operational risk to trajectory conformance, the RNP level requirement denoted here by λ is defined as a reciprocal function of ξ and three parameters, *a, b,* and *c* (4). Fig. 2 illustrates this function, where the vertical asymptote *a* sets a threshold for risk awareness - operational risk less than *a* is ignored; the horizontal asymptote *b* sets the technological limit of RNP level - i.e., *b* is the most accurate RNP level that can be achieved by UAS (equivalently, the smallest attainable TSE); and *c,* which sets the degrees of curvature, reflects the sensitivity of RNP level to a given operational risk - i.e., for the same operational risk, the RNP level requirement varies depending on *c*.

$$\lambda = \frac{c}{\xi - a} + b \quad (4)$$

The value of *a* is set based on VLOS operational constraints and current small quadrotor UAS endurance. Table 2 has the variables and their values used for the calculation of *a*, (5), with clarifying notes in the rightmost column. The implication of this value is that the risk of operating a very light UAS (about 0.25kg) in VLOS condition with only the operator of the UAS in the area is low enough to be ignored.

Table 2. Variables and values used for a

| Variable Name	Value	Note
$\rho\_vulnerability^a$	1.02E-05m^{-2}	One person, one car, and no other airspace users in circular operational area with a diameter of 250m
KE^a	249J	$MTOW$=.25kg (FAA registration exception limit [20]), V_{max}=44.7m/s (FAR Part 107 speed limit)
dT^a	1800s	Endurance of popular quadrotor small UAS

$$a = \rho\_vulnerability^a * KE^a * dT^a$$
$$= 4.58\text{J}\bullet\text{s/m}^2 \qquad (5)$$

The value of *b* is set to 3m, based on the analysis of error in the position relative to the commanded path. This analysis is based on recent studies on autonomous helicopter operations [22, 23, 24, 25].

The choice of an appropriate value for *c* is based here on a study of 19 VLOS UAS operations conducted during a test of preliminary UTM system prototype. This test took place at an inactive airfield in the middle of agricultural fields with limited habitation at Crows Landing, California, USA. Up to two spatially separated operations were concurrently conducted in the test, with single UAS flown in each operational area. Additional details of the test are available in [26]. The aspects of this test relevant to this paper are as follows:

- Most of the operations had flight durations less than 15 minutes.
- The patterns flown mimicked an area-monitoring Concept of Operations (ConOps) where a UAS is used to survey or inspect terrestrial objects.
- Notice to Airmen (NOTAM) and operational procedures were used to ensure that only the test UAS were in the test area.
- An average of eight people and four cars were in the vicinity of the operational area.

Under these operational conditions, the value of *c* is set to 1570J•s/m: this value associates the 75th percentile of risk of the 19 operations (ξ^c = 20.8J•s/m^2) with RNP level requirement of λ^c =
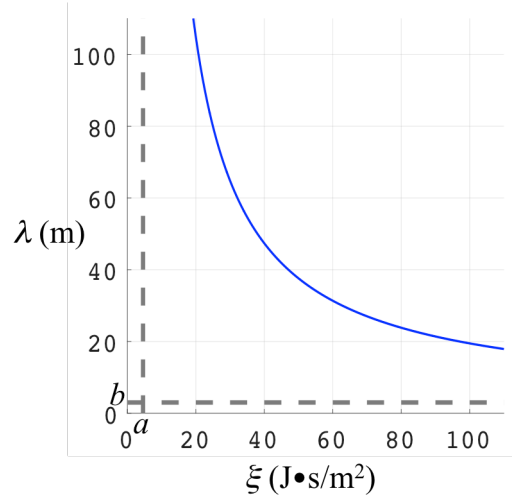
Figure 2. RNP level requirement vs. operational risk

100m (6). The implication of this value is that for an operational risk, 20.8J•s/m^2, aircraft is required to remain laterally within 100m from its planned path for 95 percent of the total trajectory.

$$c = (\lambda^c\text{-}b) * (\xi^c\text{-}a)$$
$$= (100\text{m-}3\text{m}) * (20.8\text{J}\bullet\text{s/m}^2 - 4.58\text{J}\bullet\text{s/m}^2)$$
$$= 1570\text{J}\bullet\text{s/m} \qquad (6)$$

The graph in Fig. 2 is shown with the quantified *a, b,* and *c* (7).

$$\lambda = \frac{1570}{\xi - 4.58} + 3 \qquad (7)$$

Fig. 3 shows the 95th percentile of lateral flight plan conformance error of the five multirotor UAS flown at the test, with the corresponding ξ. Each UAS has multiple values of ξ in Fig. 3 as they flew multiple operations with different durations (*dT*). Table 3 describes the legend and explanations.

Table 3. Information about Multirotor UAS operated at the UTM Event

UAS ID	$MTOW$(kg)	V_{max}(m/s)	Fig. 3 Symbol
UAS1	1.68	5	I
UAS2	3.31	5	X
UAS3	10.9	5	S
UAS4	3.99	18	D
UAS5	5.0	12.5	A
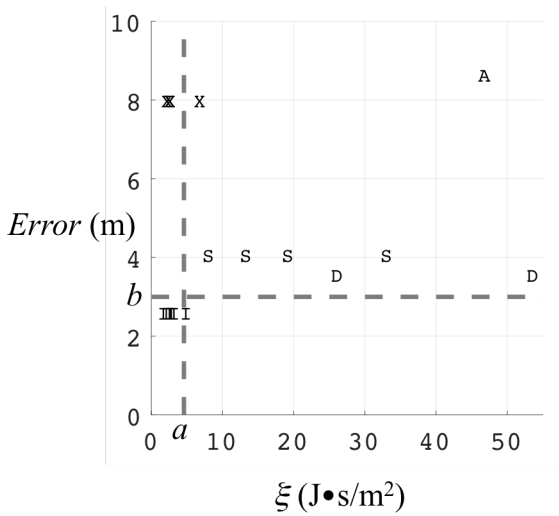
Figure 3. 95th percentile lateral flight plan conformance error vs. operational risk

Fig. 3 shows that most operations conducted by UAS1, and a few by UAS2, represented by symbols "I" and "X" respectively, carried operational risk smaller than *a*. This indicates that the risk of these operations is low enough to not require a RNP precision level. The lateral conformance errors of the remaining UAS operations were less than the RNP level requirement given by (7). However, all of these errors were calculated from the aircraft reported positions and the true positions were unknown. Therefore, there is not enough information to determine whether the required RNP levels were met.

2.3 UTM Application

The relationship (7) between operational risk and RNP level proposed in Subsection 2.2 is an initial research effort. Further refinement is required before such a relationship is ready for application in the UTM system. These refinements include the development of methods to estimate the number and distribution of people, properties, and airborne users in the operational area as time-dependent variables (i.e., to drop the assumption that $\rho\_vulnerability$ is constant). Use of additional factors other than *KE,* such as potential energy and composition of the vehicle, to define *Action* should be considered in assessing the impact of UAS on people and assets. Further research is required to determine the suitability of the formula for

computing operational risk (3) for various UAS applications.

One potential application of the relationship between operational risk and RNP level is in adjusting the RNP level based on the number of planned operations in the same area. For example, a more accurate RNP level will be required if more flights will be concurrently conducted in the same area, as this will increase ξ (i.e., increase in $\rho\_airborne\_user$ (1)). Another potential application is to adjust the RNP level that varies over time based on population density. For example, the RNP level for operations over a popular summer vacation area would be different in the summer versus the rest of the year because of changes in the number of people and cars in the town (i.e., changes in ρ_people and $\rho\_property$ (1)).

To enable the use of the RNP concept in traffic management of UAS, a method to measure UAS's achievable lateral flight path precision is needed. Operational eligibility will be determined by comparing this precision with RNP level requirement. The following Section describes a modeling and simulation approach to assessing achievable RNP levels of UAS by estimating their TSEs.

3 UAS TSE Assessment with Vehicle Modeling and Wind Field Information

3.1 Description of Approach

A largely non-homogeneous fleet of UAVs will be operating in low altitude and will likely be commercially developed. Due to intellectual property concerns, the operators may not provide detailed specifications of the control system to the UTM system. In addition, the huge variety of UAVs makes modeling each control system prohibitive and flight data for these vehicles may not exist. Therefore, the UTM system will need a generalized, simple trajectory prediction model that 1) does not rely on detailed knowledge of the control system and 2) predicts the UAV flight dynamics in the presence of urban winds, without the loss of sufficient accuracy. The output of this model

should provide a reasonable TSE for equation (7).

This section outlines the development of a simple trajectory model that simulates the performance of a quadrotor in the presence of urban wind field. It is assumed that some information from the manufacturer about the vehicle is available, such as its dimension and performance, but detailed information about its control system is not available.

The trajectory model must determine the feasibility of the vehicle's intended flight operation, given the current flight conditions and vehicle characteristics, without significant computation time. This model is not a substitute for a vehicle's control system. Rather, it must estimate the limits of a UAS's capabilities to inform the TSE assessment (assume the NSE and PDE are zero).

The requirements stated above are met by implementing a simplified trajectory model with a gain scheduled PID controller. This was selected for its simplicity and because most quadrotors control systems implement linearized models with PID controllers.

The gain table was determined using genetic optimization because this method is a gradient-free search method, immune to problems related to local optima. Thus, guaranteeing a gain solution for every run and enabling the incorporation wind field compensation in the control system. The following subsections describe the methodology.

3.1 Quadrotor Dynamics

A summary of the derivation for the equations of motion (EOMs) that describe the dynamics of a symmetric quadrotor is included. For a detailed write-up of this derivation, see [27]. One of the simplest multi-rotor small UAS configurations is a "+" configuration where positive forward motion of the vehicle is parallel with the x-axis in the body frame. Quadrotor UAS are considered to be under-actuated because they utilize four rotors to control six degrees-of-freedom.

The two major reference frames are the vehicle-fixed body frame and the Earth-fixed North-East-Up (NEU) inertial frame. The body-frame is attached to the center of gravity of the quadrotor. The NEU frame is attached to the location of the ground station tracking the vehicle.

The quadrotor is treated as a point mass with spherical aerodynamic characteristics (i.e., constant drag coefficient in all directions). Lift and nonlinear aerodynamic effects will be neglected. The model is simplified by linearizing using a small angle approximation.

The above assumptions and formulation generate the governing equations for the quadrotor as shown below.

$$\ddot{\phi} = \frac{(F_L - F_R)l}{J_X} \tag{8}$$

$$\ddot{\theta} = \frac{(F_F - F_B)l}{J_Y} \tag{9}$$

$$\ddot{\psi} = \frac{K(-F_F + F_R - F_B + F_L)l}{J_Z} \tag{10}$$

$$\ddot{X} = -\cos(\phi)\sin(\theta)\frac{F}{m} + \frac{D_X}{m} \tag{11}$$

$$\ddot{Y} = \sin(\phi)\frac{F}{m} + \frac{D_Y}{m} \tag{12}$$

$$\ddot{Z} = \cos(\phi)\cos(\theta)\frac{F}{m} - g + \frac{D_Z}{m} \tag{13}$$

where ϕ is the roll angle, θ is the pitch angle, ψ is the yaw angle, F is total force, $F_{L,R,F,B}$ are the resultant forces from each rotor (left, right, front, and back), $D_{X,Y,Z}$ are the drag force in the direction of the relative velocity, g is gravity, m is mass of the vehicle, l is the distance from the rotor to the vehicle center of gravity, $J_{X,Y,Z}$ are the moments of inertia, and K is gain of the motor that drives the rotor. Two dots above a letter (diaeresis) are used to indicate accelerations.

The set of the rotational equations (8, 9, 10) is uncoupled and depends only on the forces generated by the vehicle, whereas the translational set (11, 12, 13), depends on: the attitude angles, the total force generated by all

rotors and the applied external forces. By assuming a constant yaw of zero, the translational equations describe motion in the inertial NEU system with origin located at either a ground station or the initial position of the vehicle.

The effect of the wind field on the trajectory is determined via the drag terms in the translational EOMs.

$$\vec{U}_{wind} = u_{wind}\hat{i}_{NEU} + v_{wind}\hat{j}_{NEU} + w_{wind}\hat{k}_{NEU} \qquad (14)$$

It is assumed that the wind-generated lift is negligible and the drag coefficient/area is constant. The wind velocity vector (14) is then added to the vehicle velocity vector as follows:

$$\vec{V} = \vec{V}_{vehicle} - \mathbf{R}_b^{NEU}\vec{U}_{wind} \qquad (15)$$
$$= V_x\hat{i}_b + V_y\hat{j}_b + V_z\hat{k}_b$$

where $\vec{V}_{vehicle}$ is the vehicle velocity in the body axis and $\mathbf{R}_b^{NEU}$ is the transformation matrix from the NEU axis to the body axis. Equation (15) is included in the drag term as follows:

$$\vec{D} = -\frac{1}{2}C_D A_{ref}\rho\left[V_X^2\hat{i}_b + V_Y^2\hat{j}_b + V_Z^2\hat{k}_b\right] \qquad (16)$$

where C_D is the drag coefficient, A_{ref} is the reference area of the vehicle, and ρ is the density.

3.2 Control Methodology

The intermediate control laws for commanded total force, roll angle, and pitch angle are derived by first treating the left-hand sides of (11, 12, 13) as commanded accelerations and then solving for the commanded total force (thrust) using (13). The newly derived force equation is substituted into (11, 12) to determine the rest of the parameters:

$$F = \frac{m\left(a_Z^c + g - \dfrac{D_Z}{m}\right)}{\cos\left(\phi^c\right)\cos\left(\theta^c\right)} \qquad (17)$$

$$\phi^c = \tan^{-1}\left(\frac{\left(a_Y^c - \dfrac{D_Y}{m}\right)\cos(\theta)}{a_Z^c + g - \dfrac{D_Z}{m}}\right) \qquad (18)$$

$$\theta^c = \tan^{-1}\left(\frac{-\left(a_X^c - \dfrac{D_X}{m}\right)}{a_Z^c + g - \dfrac{D_Z}{m}}\right) \qquad (19)$$

where $a_{X,Y,Z}^c$ are the acceleration commands in the X, Y, and Z directions.

The linear equations of motion (8-13), represent the plant in the control system block diagram shown in Fig 4.

For this model, an outer-loop PID controller is used to reduce steady-state error in reaching a waypoint, and inner-loop PD controller is used to reflect the fast attitude dynamics of multi-rotor vehicles (20).

$$PID = K_p e_r + K_d\frac{de_r}{dt} + K_I\int_0^t e_r\,d\tau \qquad (20)$$

The inputs to the control system are the desired waypoints that define the operation, and the outputs are controls that drive the equations of motion to generate the desired trajectory. The inner-loop of the control system in Fig. 4 controls attitude, while the outer-loop controls vehicle position. The outer-loop system will be used to determine commanded accelerations that will in turn, determine total thrust and commanded attitude angles using Eqns. (17, 18,
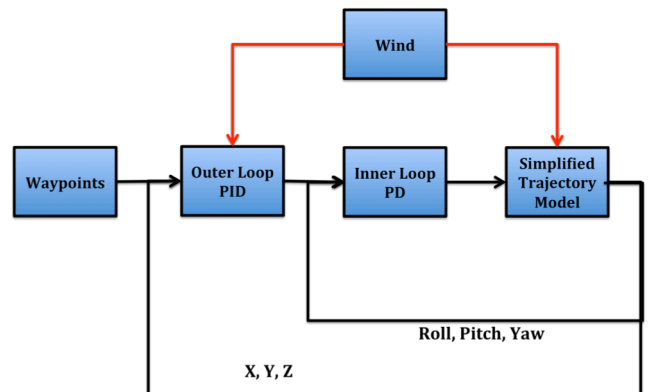

Figure 4. Quadrotor control system diagram

19). The inner-loop system will take this information and output torques to achieve an intended orientation. The integrative term, in (20), will become more influential as error accumulates, driving the vehicle closer to its intended destination. Additionally, this term adds to the vehicle's robustness to wind disturbances provided there is no degradation in stability.

The control system shown in Fig. 4 uses constant gains for the inner-loop controllers and gain scheduling in the outer loop to adapt to varying wind conditions. The gain schedule table is determined using the Artificial Bee Colony (ABC) genetic optimization method (see [28, 29]). This method is a gradient-free search method, immune to problems related to local optima. Since this trajectory model is a proof of concept, the ABC method was selected because the code was open source and successfully applied in references [28,] and [29]. A diagram from [28] is modified to illustrate this paper's implementation of the ABC method in Fig. 5.

The design variables in the optimization are the PID gains for each controller for a given wind magnitude (not for each wind component). The minimum and maximum wind magnitudes were extracted from the wind field model and gains were determined at each wind condition, in increments of $\Delta INCR = \sqrt{3}$.

$$\left[\left| \vec{U}_{wind} \right|_{min} : \Delta INCR : \left| \vec{U}_{wind} \right|_{max} \right] = \left[-5\sqrt{3} : \sqrt{3} : 5\sqrt{3} \right] \quad m/s \tag{21}$$
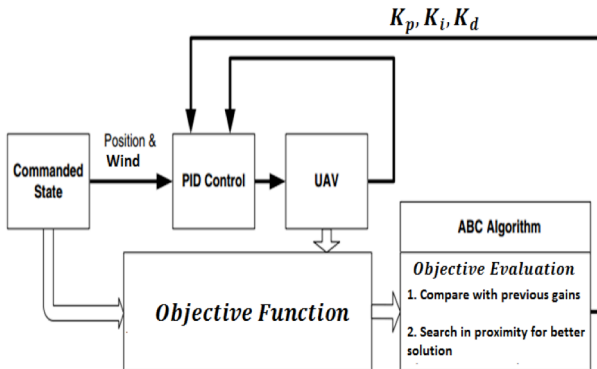

Figure 5. Block diagram of the ABC algorithm integrated with the quadrotor control system

The cost function used to find the gains at each controller is a function of six parameters and weighting coefficients. These parameters are the *TSE* at the final waypoint (*tse$_{final}$*), Integrated Time Absolute Error (*ITAE*), Percent Overshoot *(%OS)*, Rise Time (*T$_{rise}$*), Settling Time (*T$_{settling}$*) and the Number of oscillations in the trajectory (*N$_{ring}$*). The objective function, (22), is sum of these costs.

$$J_{i=X,Y,Z} = R_1 \left(tse_{final} \right)^2 + R_2 \left(ITAE \right)^2 +$$
$$R_3 \left(\%OS \right)^2 +$$
$$R_4 T_{rise} + R_5 T_{settling} + R_6 N_{ring} \tag{22}$$
$$J = J_X + J_Y + J_Z + RT_{final}$$

3.3 Vehicle and Wind Models

The test vehicle for this simulation is the AscTec Pelican Quadrotor UAS (AscTec) [30]. This vehicle is 0.651m long with a rotor diameter of approximately 25.4cm and length of 32.5cm. It has a *MTOW* of 1.65kg and a take off thrust of 36N. The specifications indicate that this vehicle can tolerate a wind speed up to 10m/s, but does not indicate whether this is a sustained wind or gust value. Based on the assumption of a spherical aerodynamic model, C$_D$ is set to a constant 0.5, with a constant A$_{ref}$ of 0.33m^2.

The flow over a single building was simulated in the open source CFD solver, OpenFOAM [1]. OpenFOAM solves the 3 dimensional (3D) incompressible Navier-Stokes equations, which provides velocity vectors at each of the discretized points in the OpenFOAM volume solution, in and around the building. OpenFOAM was chosen because it has functionality to model the Atmospheric Boundary Layer, which plays a large role in characterizing the wind field at low altitude. Fig. 6 shows the wind vectors corresponding to a cross section of the flow volume at a specific altitude, where the spectrum of red to blue wind vectors indicate high speed and low speed respectively. Using the flight dynamics model,

---

[1] www.openfoam.com

the vehicle was flown through the 3D wind field generated from OpenFOAM.

The integrated vehicle and wind field model was tested via two operational test profiles. The first test profile examines the vehicle's resilience to varying wind speeds when flying through the wake behind the building. The second test profile examines the vehicle's resilience to sustained, high wind speeds when flying near the side of the building. The flight plan segments consist of: 1) Ascent, 2) Uni-directional Forward Flight, 3) Uni-directional Backward Flight, and 4) Descent.
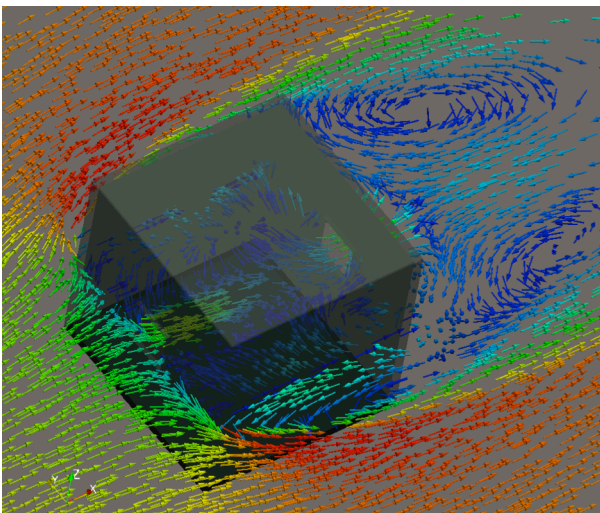
Figure 6. Altitude slice of the flow field around a single building with a window

3.4 Test Results

The results for the first test profile are shown in Fig. 7-9, and the second profile in Fig. 10-13. The first test profile shows that the system is able to maintain an altitude of 3 meters and manages to arrive at the final destination at almost the same time as the no-wind trajectory (Fig. 7). The control system also does exceptionally well at tracking the desired position with very little deviation from the no-wind path (Fig. 8). Thus, even when the wind field is constantly varying due to the wake vortices behind the building (Fig. 9), the flight path is robust to the wind variation. The corresponding TSE (RNP, λ) for this case is < 2m, based on the ground track deviations in Fig. 8. This indicates that this vehicle can fly within all operational risk scenarios, ξ (Fig. 3).

The RNP (λ) for the 2nd test profile is < 2m (Fig. 11), indicating that the vehicle can fly in all operational risk scenarios, ξ (Fig. 3). However, the vehicle requires approximately seven-times the nominal flight time to complete the trajectory (see Fig. 10) indicating that the vehicle has the potential to be carried away with wind if the sustained wind magnitudes increase
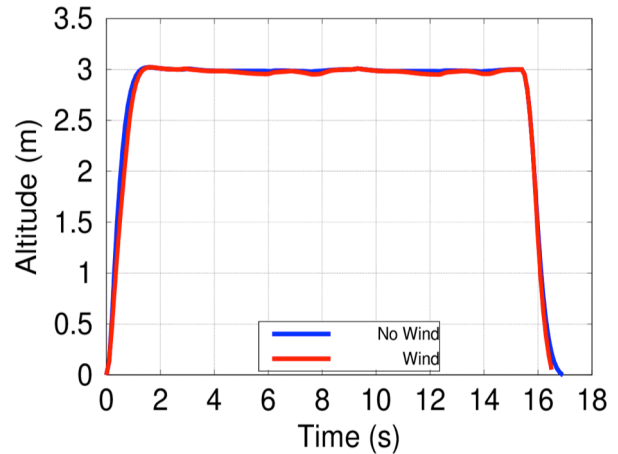

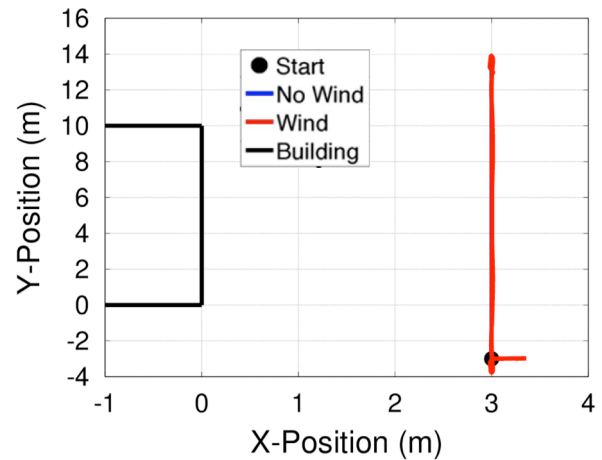**Figure 7. Altitude vs. time, 1st test profile**
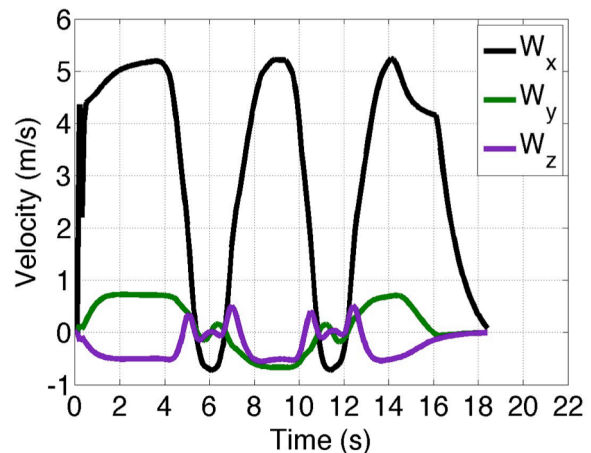

Figure 8. Ground track, 1st test profile

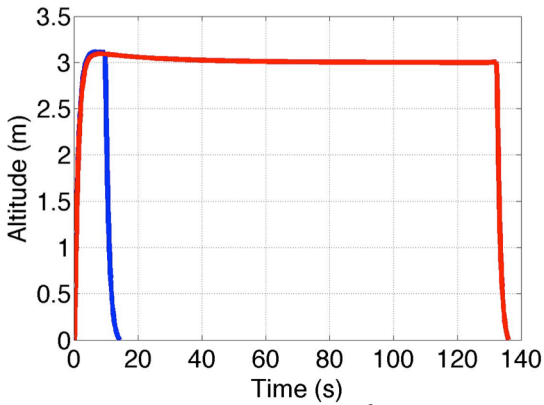**Figure 9. Magnitude of each wind components at each time point in the trajectory, 1st test profile**

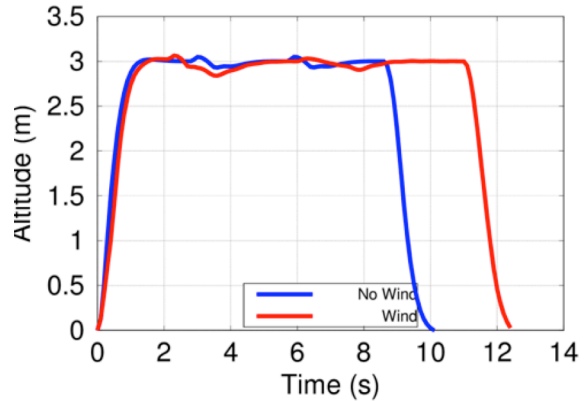**Figure 10. Altitude vs. time, 2nd test profile, with high sustained winds and small angle approximation**

Figure 11. Ground track, 2nd test profile

Figure 12. Magnitude of each wind components at each time point in the trajectory, 2nd test profile

Figure 13. Altitude vs. time, 2nd test profile, with relaxed small angle approximation

Figure 14. Ground track, 2nd test profile, with relaxed small angle approximation
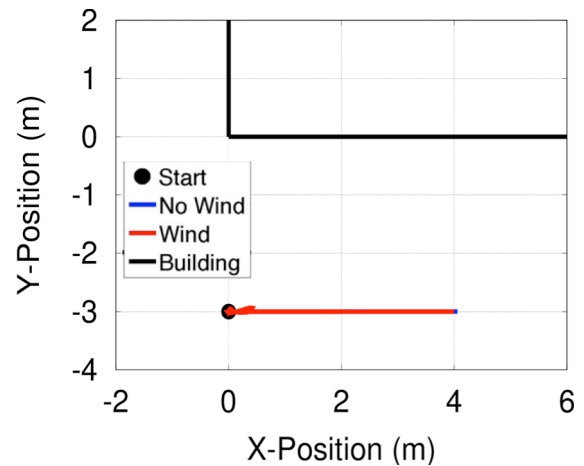
above the current conditions (Fig. 12).

The constant force of the wind on the vehicle exposes the region of poor performance in the PID. Given that typical quadrotors implement simple PID controllers, application of the RNP concept could be extended to the time dimension in a future study to incorporate

consequences of using the simple controllers in meeting arrival times to specified locations.

At this point it is important to understand the reasons for the modeled poor performance shown in Fig. 10. This will allow for further identifications of requirements on the vehicle control system to ensure robust navigation performance for safe operation. The poor performance of the controller may be due to the small angle approximation assumption applied to simplify the model. To test this, the small angle approximation was relaxed and the 2nd test profile was computed again.

The resulting altitude profile (Fig. 13) shows that the vehicle arrived at its final destination approximately two seconds later than in the no-wind condition and the ground track deviation (Fig. 14) is very small. This indicates achievable RNP level for this vehicle in the simulated wind

condition is below *b,* and it can fly within all operational risk scenarios, ξ (Fig. 3).

The effect of the small-angle assumption in the vehicle model on the vehicle performance in winds highlights the risks of linearization. The small-angle linearization restricts the maximum pitch and roll angle. As a result, the simplified model indicates that the UAS cannot safely fly in sustained wind flows with speeds greater than 5m/s. When compared with the UAS manufacturer's stated wind limitation of 10m/s, which is likely conservative, this result indicates that the equations of motion and control model need to be improved to properly reflect nonlinear dynamics. This will provide more accurate RNP information for future applications.

3.5 Future Improvement of the Model

Analyses in the previous Subsections show that a linear model of a small UAS is not sufficient for addressing the contribution of wind, when the control system is largely unknown. It was expected that the linear model would not be able to handle all non-linear effects, but this study was meant to identify the envelope of wind disturbances where the vehicle can maintain stability and control. However, the model revealed that another level of fidelity must be added in order to compensate for exposure to an urban wind field. This model was used as a starting point because the objective is to implement the simplest model and implementation of the highest fidelity would require highly detailed vehicle information.

Development of a higher fidelity generalized model should be approached on four fronts: aerodynamics, flight mechanics modeling, control system, and urban wind field modeling. First, the aerodynamics of UAS must be modeled more accurately such that the effects of the wind disturbance correctly reflect the aerodynamics in each axis. UAS also experiences aerodynamic moments and lift depending on the vehicle's configuration, e.g. '+' or 'x' configuration, for example. These forces impact how the control system maintains the vehicle's trajectory and stability. Second, UAS will not be limited to the linear region of operation as higher wind speeds and turbulent

flows will require significant fast-time changes in pitch, roll, and yaw angles for maintaining flight trajectory. Therefore, the model must account for gyroscopic and other nonlinear effects that significantly influence the total dynamics of the system. Third, the task of dealing with the wide range of nonlinear aerodynamics and dynamic effects may require a model of a nonlinear control system. This implementation will require a trade-off in fidelity since this model will need to be broadly applicable to different types of UAS, e.g. fixed wing, multirotors, etc. Finally, fidelity of the urban wind environment should be increased by including multi-building configurations and varying the inflow condition. The inflow condition is the initial condition velocity profile that corresponds to the prevailing wind speed and terrain.

To further the UAS RNP level assessment, efforts are being made to compare the modeled trajectory with actual flight trajectory. Specifically:

- Carrier Phase Differential GPS is being incorporated in small UAS to provide true position.
- A weather-sensing payload is being developed to collect three-dimensional wind information.
- A wind tunnel test has been conducted to examine aerodynamic moments and lift of small multirotor UAS [31]. Results from this test will be used to refine the vehicle EOMs.

4. Conclusions

This paper investigates an application of the Required Navigation Performance (RNP) concept for traffic management of small Unmanned Aircraft System (UAS) by relating operational risk to a trajectory conformance requirement. First, a method to quantify operational risk is introduced. Then, a reciprocal function is defined to relate greater operational risk to more accurate RNP level, or equivalently, to smaller Total System Error (TSE) requirement. Visual Line of Sight

operational constraints and data from 19 small UAS flights were used to set values of three parameters used in this function: a threshold for risk awareness, the technological limit of RNP level that can be achieved by UAS, and the sensitivity factor of RNP level to a given operational risk. One potential application of the relationship between operational risk and RNP level is in adjusting the RNP level based on the number of planned operations in the same area. Another potential application is to adjust the RNP level that varies over time based on population density. To enable such applications, the vehicles' RNP level information is needed. Simulation results showed that the vehicle model and Computational Fluid Dynamics generated wind field information could be used to assess achievable RNP level of UAS, but further development of a more generalized model is needed to properly incorporate nonlinear dynamics for determining UAS RNP levels with increased accuracy.

References

[1] World Unmanned Aerial Vehicle Systems: 2015 Market Profile and Forecast (12th ed.). Teal Group Corporation, 2015.

[2] Skrzypietz, T. Unmanned Aircraft Systems for Civilian Missions. Brandenburg Institute for Society and Security, BIGS Policy Paper No. 1, 2012.

[3] Quater, P. B. et al. Light Unmanned Aerial Vehicles for Cooperative Inspection of PV Plants. *IEEE Journal of Photovoltaics,* 4(4), pp 1107-1113, 2014.

[4] Giles, D. K. and Billing, R. C. Deployment and Performance of a sUAS for Crop Spraying. *Chemical Engineering Trnsactions,* 44, pp 307-312, 2015.

[5] Irizarry, J. and Johnson, E. N. Feasibility Study to Determine the Economic and Operational Benefits of Utilizing Unmanned Aerial Vehicles (sUASs). Georgia Institute of Technology, 2014.

[6] Kimchi, G. et al. Unmanned Aerial Vehicle Delivery System. US Patents, US20150120094 A1, 2015.

[7] Clarity from Above PwC Global Report on the Commercial Applications of Drone Technology. PricewaterhouseCoopers, 2016.

[8] CES 2016 Guide to Drones. Consumer Technology Association, 2016.

[9] Operation and Certification of Small Unmanned Aircraft Systems. FAA, 2016.

[10] Unmanned Aircraft System (UAS) Service Demand 2015-2035: Literature Review and Projections of Future Usage (Version 0.1). John A. Volpe National Transportation Systems Center, 2013.

[11] FAA Aerospace Forecast: Fiscal Years 2015-2035. FAA, 2015.

[12] Unmanned Aircraft System (UAS) Traffic Management (UTM) Fact Sheet. NASA, Retrieved May 25, 2016 from http://utm.arc.nasa.gov/docs/utm-factsheet-02-23-16.pdf.

[13] Kopardekar, P. et al. Unmanned Aircraft System Traffic Management (UTM) Concept of Operations. 2016 *AIAA Aviation Forum and Exposition,* Washington, DC. 2016.

[14] Performance-based Navigation (PBN) Manual. International Civil Aviation Organization, Doc-9613, AN/973, 2008.

[15] Aeronautical Information Manual. FAA, 2015.

[16] Required Navigation Performance 10 (RNP 10) Operational Authorization. FAA, Order 8400.12c, 2011.

[17] Integration of Civil Unmanned Aircraft System (UAS) in the National Airspace System (NAS) Roadmap. FAA, First edition, 2013.

[18] System Safety Handbook. FAA, Chapter 15, 2000.

[19] Clothier, R.A. and Walker, R. A. Safety Risk Management of Unmanned Aircraft Systems. *Handbook of Unmanned Aerial Vehicles,* Valavanis, K. P. and Vachtsevanos, G. J., editors, pp 2229-2275, Springer, 2014.

[20] Unmanned Aircraft System (UAS) Registration, http://www.faa.gov/uas/registration/ [cited Jun. 2016]

[21] Encyclopedia Britannica, http://www.britannica.com/science/action-physics [cited Jul. 2015]

[22] Takahashi, M. D. et al. Development and Flight Testing of Fight Control Laws for Autonomous Operations Research on the RASCAL JUH-60A. The American Helicopter Society (AHS) 68th Annual Forum, Fort Worth, Texas, 2012.

[23] Takahashi, M. D., Schulein, G. and Whalley, M. Flight Control Law Design and Development for an Autonomous Rotorcraft. The AHS 64th Annual Forum, Montreal, Canada, 2008.

[24] Goerzen, C. and Whalley, M. Minimal Risk Motion Planning: a New Planner for Autonomous UAVs in Uncertain Environments. The AHS Specialists' Meeting on Unmanned Rotorcraft, Tempe. Arizona, 2011.

[25] Whalley, M., Takahashi, M. D., Schulein, G., and Goerzen, C. Field-Testing of a Helicopter UAV obstacle Field Navigation and Landing System. The AHS 65th Annual Forum, Grapevine, Texas, 2009.

[26] Johnson, M. A. et al. Flight Test Evaluation of a Traffic Management Concept for Unmanned Aircraft System in a Rural Environment. NASA TM, To be published.

[27] Beard, R. "Quadrotor Dynamics and Control," Brigham Young University. (2008) http://rwbclasses.groups.et.byu.net/lib/exe/fetch.php?media=quadrotor:beardsquadrotornotes.pdf

[28] Abachizadeh, M., et al., Optimal Tuning of PID Controllers Using Artificial Bee Colony Algorithm. *2010 IEEE/ASME International Conference on Advanced Intelligent Mechatronics,* Montreal, Canada, 2010.

[29] Ghiglino, P., et al. Online Evolutionary Swarm Algorithm for Self-Tuning Unmanned Flight Control Laws. *Journal of Guidance, Control, and Dynamics,* Vol. 38, No. 4, pp. 772-782, 2015.

[30] AscTec Pelican Safety Data Sheet." Ascending Technologies. Web. 18 Sept. 2014. http://www.asctec.de/downloads/datasheets/AscTec-Pelican_Safetydatasheet.pdf

[31] Russell, C., Jung, J., Willing, G., and Glasner, B. Wind Tunnel and Hover Performance Test Results for Multicopter UAS Vehicles. The AHS 72nd Annual Forum, West Palm Beach, Florida, 2016.

Contact Author Email Address

mailto: jaewoo.jung@nasa.gov

Copyright Statement